Combustion, Explosion, and Shock Waves, Vol. 42, No. 4, pp. 436–449, 2006

Condensed Combustion Products of Aluminized Propellants. IV. Effect of the Nature of Nitramines on Aluminum Agglomeration and Combustion Efficiency

O. G. Glotov[1]

UDC 536.46

Translated from *Fizika Goreniya i Vzryva*, Vol. 42, No. 4, pp. 78–92, July–August, 2006.
Original article submitted July 5, 2004; revision submitted March 6, 2006.

The condensed combustion products of two model propellants consisting of ammonium perchlorate, aluminum, nitramine, and an energetic binder were studied by a sampling method. One of the propellants contained HMX with a particle size $D_{10} \approx 490$ μm, and the other RDX with a particle size $D_{10} \approx 380$ μm. The particle-size distribution and the content of metallic aluminum in particles of condensed combustion products with a particle size of 1.2 μm to the maximum particle size in the pressure range of 0.1–6.5 MPa were determined with variation in the particle quenching distance from the burning surface to 100 mm. For agglomerates, dependences of the incompleteness of aluminum combustion on the residence time in the propellant flame were obtained. The RDX-based propellant is characterized by more severe agglomeration than the HMX-based propellant — the agglomerate size and mass are larger and the aluminum burnout proceeds more slowly. The ratio of the mass of the oxide accumulated on the agglomerates to the total mass of the oxide formed is determined. The agglomerate size is shown to be the main physical factor that governs the accumulation of the oxide on the burning agglomerate.

Key words: aluminized propellant, HMX, RDX, agglomeration, condensed combustion products, completeness of aluminum combustion, evolution of agglomerates.

INTRODUCTION

Metal (aluminum) and energetic materials (in particular, RDX or HMX) are added to rocket propellants to increase the specific impulse [1, 2]. For example, the composition of the rocket propellants subject to destruction under the Strategic Arms Limitation Treaty (SALT) is as follows: 46% ammonium perchlorate (AP), 20% aluminum, 25% HMX, and 9% binder [3]. The RDX and HMX cyclic nitramines are not only energetic but are also characterized by high density, thermal stability [4], and compatibility with the conventional components of solid rocket propellants [5]. Nitramine-based propellants are considered less smoky and more eco-friendly because of the lower content of AP. The use of RDX and HMX in propellant formulations has motivated their comprehensive study (see, for example, surveys [6–8], special issues of the *Journal Propulsion and Power* [9, 10], numerous articles in the Proceedings of the International Annual Conference of the Institute for Chemical Technology (Karlsruhe, Germany). Most papers, including recent reports [11–16], which were not considered in the above-mentioned surveys, are concerned with studies of these nitramines as individual substances. Much less attention has been given to the combustion of nonmetallized nitramine-based propellants [17–19] and the combustion of aluminized nitramine-based propellants [20–26]. Experimental data from [21–24] will be invoked in the discussion of results below.

In the present work, the condensed combustion products (CCPs) of two model aluminized propellants — an RDX-based propellant and an HMX-based propellant — were studied by a sampling method. Emphasis was on the characteristics of the coarse fraction

[1]Institute of Chemical Kinetics and Combustion, Siberian Division, Russian Academy of Sciences, Novosibirsk, 630090; glotov@ns.kinetics.nsc.ru.

 0010-5082/06/4204-0436

TABLE 1

Model Propellant Formulations

Propellants	Mass content, %					
	AP1 $S_{sp} = 6000$ cm^2/g	AP2 200–315 μm	HMX 250–700 μm	RDX 250–700 μm	Aluminum 10–30 μm	Binder (98%) + additives (2%)
E12	7	18	35	—	20	20
R	7	18	—	35	20	20

Notes. The AP2, HMX, and RDX particles are sieved fractions. The metallic aluminum content determined by a permanganometric method [30] is 99.5%. The energetic binder is based on butadiene nitrile polymer plasticized with diethylene glycol dinitrate.

TABLE 2

Mean Sizes D_{mn} of Powder Propellant Components

Component	Analysis method	D_{10}	D_{20}	D_{30}	D_{43}	D_{53}
		μm				
Al	Malvern-3600E automatic granulometer	9.7	11.0	12.6	22.3	26.4
AP1	—//—	4.3	4.0	5.1	17.1	22.9
AP2	Microscope	284	288	292	306	310
HMX	—//—	486	503	522	601	621
RDX	—//—	375	378	381	397	402

Note. From the given mean sizes, it is possible (if necessary) to calculate the other statistical parameters, for example, $\sigma^2 = D_{20}^2 - D_{10}^2$, $D_{21} = D_{20}^2/D_{10}$, $D_{32} = D_{30}^3/D_{20}^2$, etc.

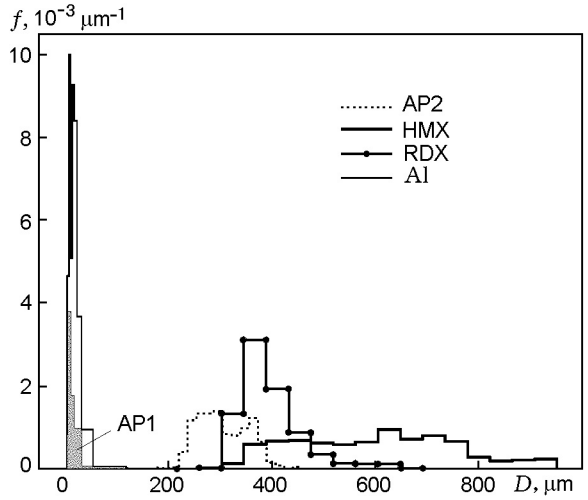

Fig. 1. Particle-size composition of the powder propellant components: the ordinate shows the size distribution density of the relative mass normalized by the mass fraction of the given component in the propellant, so that the area under the curve is proportional to the mass of the corresponding component.

of CCP — agglomerate particles. The agglomerate size determines the macrokinetics of aluminum burnout and eventually the effectiveness of using aluminum in terms of the metal combustion completeness. A comparison of the propellant parameters with the replacement of RDX by HMX is of interest due to practical applications of both nitramines.

EXPERIMENTS AND TREATMENT OF RESULTS

Propellants, Samples, and Experimental Conditions

The E12 and R model propellants [2] investigated in this study differed only in the type of nitramine (HMX or RDX); the other components and their ratios were identical (see Table 1). The powder components were subjected to particle-size analysis as is described in [29], and the results are presented in Fig. 1 and Table 2. The 250–700 μm fractions of HMX and RDX were extracted on the same sieves. However, because of the large width of the fraction and the different particle shape (Fig. 2), the grain-size characteristics of HMX and RDX differed significantly (see Fig. 1 and Table 2).

The samples were cut from a cured propellant mass in the shape of cylinders 10 mm high and 7 or 11.5 mm in diameter. The cylinders were embedded in Plexiglas cans, which served as the inhibiting layer for the lateral surface.

Combustion of the samples and sampling of CCPs were implemented using the technique and setup of [29] (a blow-through bomb with particle quenching in a

[2] The notation of [27, 28] is used.

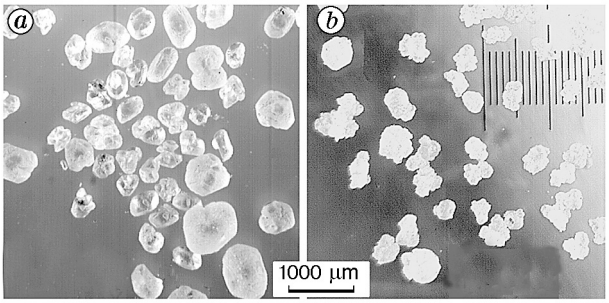

Fig. 2. View of HMX (a) and RDX (b) particles with a size of 250–700 μm.

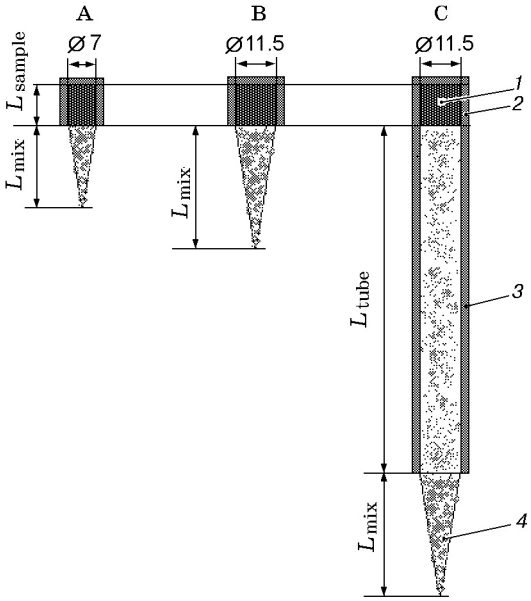

Fig. 3. Versions of the experiment geometry for changing the time of residence of agglomerates in the flame: 1) propellant sample; 2) Plexiglas can with a depth equal to the sample length L_{sample}; 3) protective Plexiglas tube of length L_{tube}; 4) initial mixing area with length L_{mix}; the sizes are in mm.

cocurrent flow of an inert gas and subsequent catching on wire mesh screens and an aerosol filter) in nitrogen at three pressure levels. At a pressure $p = 0.1$ MPa, the nitrogen was motionless; at $p \approx 2.5$ and $\approx$6.5 MPa, the nitrogen mass flow through the bomb was 1.1–2.0 and 1.8–2.0 g/sec, respectively.

Two or three samples of diameter 11.5 mm or five or six samples of diameter 7 mm were burned under identical conditions, so that the total mass of the burned propellant in a series was $\approx$3–6 g and the mass of the CCPs was 1–2 g.

To change the time of residence of agglomerates in hot products of propellant combustion, i.e., the time of agglomerate combustion before quenching, we used three geometry versions (Fig. 3):

Geometry	L_{sample}	L_{tube}	L_{mix}
A	10	–	$\approx$20
B	10	–	$\approx$30
C	10	100	$\approx$30

Representation of Results. Definitions of Parameters

The sampled CCP particles were sieved and subjected to particle-size and chemical analyses, as is described in [29, 30]. The results were plotted as a histogram $f(D)$ of the size distribution density of the relative mass of CCP particles and as a conditional histogram $f^{Al}(D)$ of the size distribution density of the relative mass of unburned aluminum in the CCP particles:

$$f_i(D) = m_i/M_{prop}\Delta D_i, \quad f_i^{Al}(D) = f_i(D)\varepsilon_j^{Al}.$$

Here D is the particle size (diameter), m_i is the mass of the particles in the ith histogram interval, M_{prop} is the propellant mass (the total mass of the samples in a series), ΔD_i is the width of the ith histogram interval, ε_j^{Al} is the mass fraction of unburned aluminum in the fraction j within which the ith histogram interval falls. Below, the subscript i is omitted, and the functions $f(D)$ and $f^{Al}(D)$ will be called mass distributions for brevity.

The minimal agglomerate size D_L that differentiates small-size particle and large agglomerate particles was determined as the size at which the mass distribution of CCPs has a local minimum, $f(D) \approx 0$. For propellants with severe agglomeration (which include the propellants studied, as will be shown below) the determination of the size D_L in such a way is natural and easy [27]. Below, particles with sizes $D < D_L$ will be called small-size particles and particle with $D > D_L$ agglomerates.

The agglomerate size distributions were quantitatively characterized by a set of mean sizes D_{mn} [29] calculated in the range D_L–D_R. Here D_R is the conditional largest agglomerate size starting with which the mass distribution $f(D)$ loses continuity (histogram intervals appear that do not contain particles).

The functions $f(D)$ and $f^{Al}(D)$ were used to calculate a number of integral parameters for the entire range of the particle sizes, separately for small-size particles and for agglomerates. The parameters were rendered dimensionless by dividing by the propellant mass.

TABLE 3

Metallic Aluminum Content in Sieved Fractions of CCPs

p, MPa	Geometry	Mass content in fractions [%]						
		<130 μm	130–300 μm	300–450 μm	450–600 μm	600–900 μm	900–960 μm	>960 μm
E12 propellant								
0.1	A	1.76 ± 0.14	49.2 ± 0.2	46.8 ± 1.0	53.1 ± 0.9	46.9	49.3	
0.1	B	0.49 ± 0.02	51.2 ± 0.2	45.0 ± 0.3	41.6 ± 1.0	36.4	≅40.2	No fraction
0.1	C	2.3 ± 0.1	45 ± 2	44.8 ± 0.1	45.0 ± 1.5	39.9	24.6	
2.2	A	0.30 ± 0.06	47.8 ± 0.5	47.8 ± 1.3	≅47.3	≅40	33.7	
2.4	B	1.20 ± 0.03	45.7 ± 0.5	49.9 ± 0.3	≅44.5			
2.4	C	0.93 ± 0.06	38.0 ± 0.2	40.9 ± 0.2	≅36.8	≅27	≅27	
6.4	A	0.46 ± 0.04	22.8 ± 1.0	37.0 ± 0.4	≅27.0	≅26.3	≅27.5	
6.6	B	0.87 ± 0.08	26.6 ± 1.6	34.9 ± 0.1	≅26.8	≅29	≅10.6	
6.7	C	0.47 ± 0.02	23.8 ± 0.1	30.4 ± 0.1	≅24.4	≅23.2	27.2	
R propellant								
0.1	A	0.83 ± 0.02	46.4 ± 0.8	41.3 ± 0.9	38.0 ± 0.1	36.8 ± 0.4	31.1	37.1
0.1	B	1.36 ± 0.01	49 ± 2	42.9 ± 0.2	38 ± 2	37.5 ± 0.5	36.6 ± 0.5	38.1 ± 0.9
0.1	C	0.82 ± 0.02	50.0 ± 0.7	42 ± 2	34.5 ± 0.1	35.8 ± 0.4	31.2 ± 0.7	31 ± 3
2.3	A	0.34 ± 0.01	44.4 ± 0.6	40.6 ± 0.7	41.5 ± 0.1	39.5 ± 0.8	≅9	
2.5	B	0.33 ± 0.04	43 ± 2	45.0 ± 0.1	42.2 ± 0.1	24.2 ± 0.1	≅9	No fraction
2.5	C	0.36 ± 0.02	36.8 ± 0.4	33.8 ± 0.2	34.2 ± 0.2	34.2 ± 0.2	≅26	29.8
6.5	A	0.77 ± 0.01	35.5 ± 0.1	33.5 ± 0.4	32.9 ± 0.4	30.0		
6.6	B	0.96 ± 0.01	27.3 ± 0.3	30.9 ± 0.3	33.3 ± 0.3	27.1	≅2.1	
6.7	C	0.34 ± 0.01	15.4 ± 0.2	17.8 ± 0.1	20.3 ± 0.5	18.0	15.7	

Notes. 1) The merging of table cells corresponds to the merging of fractions of small mass before the analysis. 2) In most cases, the mean values of two to four independent determinations are given. If the standard error is not indicated, this means that the mass of the fraction is small and the analysis was performed only once. 3) The ≅ sign denotes a low analysis accuracy due to the small mass of the fraction.

For example, the dimensionless mass of agglomerates is $m_{\rm ag} = M_{\rm ag}/M_{\rm prop}$, where $M_{\rm ag}$ is the mass of agglomerates and $M_{\rm prop}$ is the propellant mass.

In the present study, we use the following parameters: m_f is the mass of small-size particles, $m_f^{\rm Al}$ is the mass of the unburned aluminum in small-size particles, $m_{\rm ag}$ is the mass of agglomerates, $m_{\rm ag}^{\rm Al}$ is the mass of unburned aluminum in agglomerates, $m_{\rm CCP} = m_f + m_{\rm ag}$ is the total mass of CCP, $m_{\rm CCP}^{\rm Al} = m_f^{\rm Al} + m_{\rm ag}^{\rm Al}$ is the total mass of unburned aluminum in CCP, $m_{\rm prop}^{\rm Al}$ is the initial mass of aluminum in the propellant ($m_{\rm prop}^{\rm Al} \equiv 0.20$), $m_{\rm CCP}^{\rm Al}/m_{\rm prop}^{\rm Al}$ is the total incompleteness of aluminum combustion, $m_f^{\rm Al}/m_{\rm prop}^{\rm Al}$ is the incompleteness of aluminum combustion in small-size particles, $\eta = m_{\rm ag}^{\rm Al}/m_{\rm prop}^{\rm Al}$ is the incompleteness of aluminum combustion in agglomerates, $\xi = 1 - \eta$ is the completeness of aluminum combustion in agglomerates, and $\varphi = 1/[1 + (m_f - m_f^{\rm Al})/(m_{\rm ag} - m_{\rm ag}^{\rm Al})]$ is the ratio of the mass of the oxide accumulated on agglomerates to the total mass of the oxide formed.

Estimate of the Residence Time of Particles in the Flame

The residence time $t_{\rm res}$ of agglomerates in the flame was calculated using the procedure described in [29]. This time was treated as the combustion time, assuming that the particles quenched instantaneously at a distance $L_{\rm mix}$ from the edge of the can or the protective

TABLE 4

Burning Rate and Mean Agglomerate Sizes D_{mn} Calculated in the Range D_L–D_R versus Combustion Conditions

p, MPa	Geometry	r, mm/sec	D_L–D_R, μm	D_{10}	D_{20}	D_{30}	D_{43}	D_{53}
				μm				
E12 propellant								
0.1	A	1.0±0.1	119–800	260	280	302	405	430
0.1	B		119–779	275	294	314	404	426
0.1	C		127–806	252	269	288	380	405
2.2	A	7.9±1.8	87–790	238	249	260	311	325
2.4	B		95–771	234	243	253	301	316
2.4	C		87–662	222	231	241	290	306
6.4	A	13±2	127–671	225	234	244	286	297
6.6	B		119–671	207	215	224	272	288
6.7	C		44–696	223	234	246	303	320
R propellant								
0.1	A	1.0±0.1	55–1978	331	383	445	800	889
0.1	B		55–2087	317	368	433	807	907
0.1	C		55–2081	304	350	409	755	846
2.3	A	6.2±0.5	55–1385	300	328	357	499	538
2.5	B		24–1329	303	329	356	487	525
2.5	C		11–1382	301	329	360	502	540
6.5	A	10±2	55–1017	282	306	330	444	473
6.6	B		24–1343	270	288	308	400	429
6.7	C		18–1581	305	325	347	457	496

Note. The absolute error of D_{mn} is ±(22–40) μm (depending on the size), and is due to the accuracy of microscopic measurements of the particles [29].

tube (see Fig. 3). Quantity L_{mix} is the length of the initial mixing segment of coaxial turbulent jets — the flow of combustion products escaping from the sample and the ambient diluent gas. The time t_{res} was considered equal to the half-sum of the times required to travel the distance $L_{tube} + L_{mix}$ and the distance $L_{sample} + L_{tube} + L_{mix}$, thus taking into account the change in the start point of the particles due to the displacement of the burning surface. The times were determined by solving the problem of the motion of a spherical particle under gravity and Stokes forces (the drag coefficient in the form $C_d = 24/\mathrm{Re}$). The calculations performed in the present study had the following features compared to [29].

• The gas-phase parameters (temperature T_{gp}, molar mass M_{gp}, and dynamic viscosity μ) were found by thermodynamic calculations of the equilibrium composition of the combustion products with the ASTRA code. The calculations were performed for each series of experiments taking into account that a certain mass of the can and the protective tube material (Plexiglas) burned together with the propellant sample. The mass of burned Plexiglas was determined by weighing before and after each experiment. The presence of Plexiglas combustion products changes the gas parameters. For example, for the combustion products of E12 propellant at $p = 6.7$ MPa, calculations give $T_{gp} = 3772$ K, $M_{gp} = 19.9$, and $\mu = 0.82 \cdot 10^{-4}$ Pa·sec, whereas with the use of a 100-millimeter tube (geometry C), about 0.9 g of Plexiglas burned together with ≈3.4 g of the propellant and the gas parameters became $T_{gp} = 2433$ K, $M_{gp} = 18.1$, and $\mu = 0.59 \cdot 10^{-4}$ Pa·sec.

• The mean diameter D_{30} determined in geometry A was used as the particle size.

• Taking into account the experimental data, the particle density was set equal to 2.16 g/cm^3.

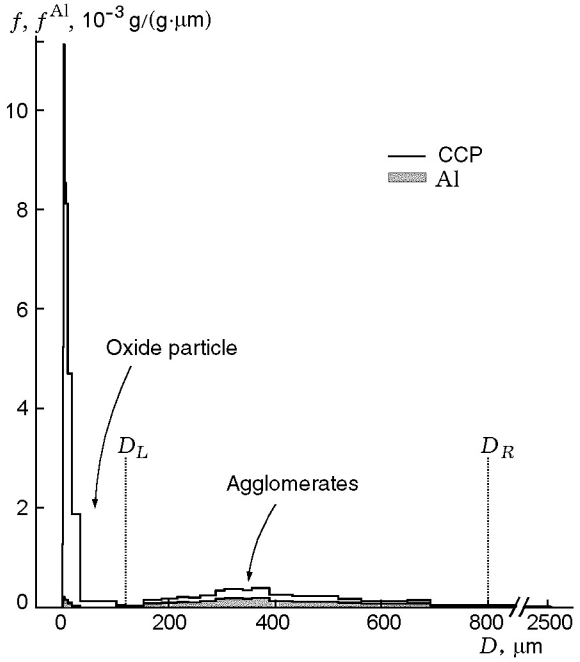

Fig. 4. Mass distributions of CCPs and unburned aluminum in CCPs (shadowed region) over sizes in the range of 0.5 μm to the maximum value: E12 propellant, $p = 0.1$ MPa, and geometry A; the size D_L is the left boundary of the distribution of agglomerates (the conditional boundary between oxide particles and agglomerates) and the size D_R is the right boundary of the distribution of agglomerates.

EXPERIMENTAL RESULTS AND DISCUSSION

Agglomeration Scenario and Agglomerate Size

Results of determinations of unburned aluminum contents in individual fractions of CCPs are presented in Table 3, the mean agglomerate sizes $D_{\rm mn}$ in Table 4, and integral mass parameters in Table 5.

Figure 4 gives examples of particle mass distributions of CCP and unburned aluminum in the CCPs of E12 propellant for the case of quenching near the surface at $p = 0.1$ MPa.

The data of Table 3–5 demonstrate that the behavior of the propellants studied follows the scenario of severe aluminum agglomeration [27, 28], which is characterized by the following features.

• The agglomerates have large sizes. In the example in Fig. 4, $D_{\max} = 2540$ μm. In this case, the mass of the CCPs is almost entirely in the range from 0 to $D_R = 800$ μm and only a small number of large agglomerates have sizes $D > D_R$.

• The mass distribution density $f(D)$ has a local minimum that separates small-size particles and agglomerates (in Fig. 4, $D_L = 119$ μm).

• The unburned aluminum content in small-size particles is low, so that they are predominantly oxide particles. In all cases, CCP particles finer than 130 μm contain not more than 2% of unburned aluminum (see Table 3). In small-size particles, the mass of unburned aluminum $m_f^{\rm Al}$ (column 7 in Table 5) is much smaller than the entire mass of unburned aluminum $m_{\rm CCP}^{\rm Al}$ (column 4). Unburned aluminum is present mainly in agglomerates, so that the mass ratio of unburned aluminum in agglomerates ($m_{\rm ag}^{\rm Al}$) and in small-size particles ($m_f^{\rm Al}$) varies from 99 : 1 to 95 : 5 (column 13 in Table 5). This allows the aluminum combustion efficiency to be characterized by the combustion completeness of the agglomerates ξ.

Let us compare the parameters of CCPs near the surface (sampling in geometry A). The data of Table 4 demonstrate that for E12 propellant, the mean agglomerate size is $D_{43} = 290$–405 μm and for R propellant, it is much larger (444–800 μm). For R propellant, the mass of agglomerates is larger ($m_{\rm ag} = 0.16$–0.20 and 0.11–0.17 for R and E12 propellants, respectively; see column 9 in Table 5), and in most cases (except at $p = 0.1$ MPa), they contain more unburned aluminum ($m_{\rm ag}^{\rm Al} = 0.07$ and 0.03–0.05 for R and E12 propellants, respectively; see column 10 in Table 5). For E12 propellant, at $p = 2.5$ and 6.5 MPa, the mass ratios of agglomerates to small-size particles are 30 : 70 (at $p = 2.5$ MPa) and 32 : 68 (at $p = 6.5$ MPa), and for R propellant, they are 46 : 54 (at $p = 2.5$ MPa) and 57 : 43 (at $p = 6.5$ MPa) (see column 12). The data collection provides strong evidence for more the severe agglomeration in the case of R propellant.

We note that in the literature there are data that RDX can cause more severe agglomeration than HMX (for example, for Al–HTPB–AP–nitramine propellants [21]). For E12 and R propellants, the agglomerate size is on the average larger than that for the nitramine-based propellants in [22–24], where $D_{43} = 190$–510 μm. However, in [21–24], the propellants contained the inert binder hydroxyl-terminated polybutadiene (HTPB), whereas the propellants used in the present study contained an energetic binder based on polybutadiene nitrile rubber plasticized with diethylene glycol dinitrate (DEGDN). It has been established [32] that the nature of the binder can have a significant effect on agglomeration. Thus, the replacement of the inert binder isoprene rubber + transformer oil by the indicated energetic binder reduces agglomeration, but partial replacement of AP by HMX in the propellant containing this binder enhances agglomeration [27, 28]. In fact, one can

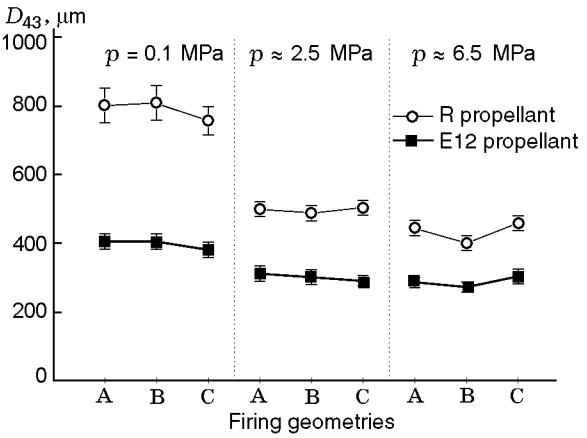

Fig. 5. Comparison of the mean agglomerates size D_{43} for E12 and R propellants sampled at different pressures and firing geometries.

argue that the combination of HMX with the binder based on polybutadiene-nitrile rubber and DEGDN is unfavorable.

Another feature that distinguishes the propellant formulations in the present study from that in [21–24] is the large mass fraction (35%) of coarse nitramine ($D_{10} \approx 490$ μm for HMX and $D_{10} \approx 380$ μm for RDX). Therefore, one might expect that the combustion of E12 and R propellants would involve severe agglomeration, but its quantitative characteristics and their change due to the replacement of HMX by RDX cannot be predicted without experiments.

For both E12 and R propellants, there is a trend toward agglomerate size reduction with pressure, which is more pronounced for R propellant (see Fig. 5). In all cases, the agglomerate size D_{43} is larger for the RDX-based propellant than for the HMX-based propellant, despite the inverse ratio of the particle sizes of RDX and HMX. The variation in the agglomerate size with pressure is usually related to the burning rate. Indeed, the higher the burning rate, the thinner the heated propellant layer and the smaller the residence time of aluminum particles in this layer. However, at $p = 0.1$ MPa, the burning rates of E12 and R propellants are close ($r \approx 1$ mm/sec), but the agglomerate sizes D_{43} in geometry A are 405 and 800 μm, respectively. This indicates the influence of factors other than the geometric structure of the propellants and the burning rate.

In [23], for AP–Al–HTPB–nitramine propellants, the following correlation among the agglomerate size D_{43} [μm], the burning rate r [mm/sec], and the mass contents of AP in the propellant $\alpha_{\rm AP}$ was proposed: $D_{43} = 118.8/r\alpha_{\rm AP}^2 + 146.5$. This relation adequately (the coefficient of determination[3] $R^2 = 0.575$) approximates the entire population of data [22, 23] (83 points for the HMX- and RDX-based propellants in the following range of parameters: nitramine content 0–20%, AP content 54–71%, and Al content 16–20%; $r = 3.4$–14.5 mm/sec). E12 and R propellants do not obey this relation, apparently because of their formulations (35% coarse nitramine and an energetic binder). For both propellants, however, there is a correlation between the value of $1/r$ and the agglomerate size D_{43}.

The geometric structure of the propellants studied can be represented as nitramine particles in contact with each other (the largest-size powder component), between which there is a binder filled with aluminum and AP particles of smaller size. Following [2], we assume that the nitramine particles and the filled binder burn at their own rates and that the burning rate of the propellant is the average of these rates. The burning rate of pure nitramines (Table 6) at corresponding pressures is lower than the burning rate of the propellants studied here (see Table 4), which indicates the determining role of the burning rate of the binder filled with AP and Al particles. According to the data of [34] (see Table 6), for combustion of pure nitramines at $p = 0.2$–0.7 MPa, the thickness of the molten layer is 20–15 μm, and at $p = 0.1$ MPa, it is 70 μm for HMX and 120 μm for RDX. For combustion of nitramines in E12 and R propellant formulations, this thickness can be smaller since the burning rate of the propellants is higher than that for nitramines. In any case, the thickness of the molten layer is a fraction of the particle diameter. The nitramine particles can protrude above the burning surface and be partially ejected. This is confirmed by the presence of such particles among the sampled CCP particles. As a result, the formation of large agglomerates in combustion of E12 and R propellants cannot be explained by the presence of a molten nitramine layer, as is done in [23] for propellants containing nitramines with a particle size of 20–255 μm.

Burnout and Evolution of Agglomerates

Figure 6 shows curves of the incompleteness of aluminum combustion versus the residence time of agglomerates in the flame. Figure 7 shows examples of mass distributions of agglomerates sampled in different combustion geometries at $p \approx 2.4$ MPa. The mean agglomerate sizes are given in Table 4, and the behavior of the mean sizes D_{43} is illustrated in Fig. 5.

[3]For a definition of the coefficient of determination see, for example, [33].

TABLE 5

Integral Mass Parameters Calculated from the Size Distribution Functions of the Mass of CCPs and Aluminum in CCPs

p, MPa	Geometry	m_{CCP}	$m_{\text{CCP}}^{\text{Al}}$	$m_{\text{CCP}}^{\text{Al}}/m_{\text{prop}}^{\text{Al}}$	m_f	m_f^{Al}	$m_f^{\text{Al}}/m_{\text{prop}}^{\text{Al}}$	m_{ag}	$m_{\text{ag}}^{\text{Al}}$	$m_{\text{ag}}^{\text{Al}}/m_{\text{prop}}^{\text{Al}} = \eta$	$m_{\text{ag}} : m_f$	$m_{\text{ag}}^{\text{Al}} : m_f^{\text{Al}}$	φ
1	2	3	4	5	6	7	8	9	10	11	12	13	14
E12 propellant													
0.1	A	0.318	0.084	0.422	0.150	0.002	0.013	0.168	0.082	0.409	53:47	97:3	0.37
0.1	B	0.307	0.071	0.354	0.153	0.001	0.004	0.154	0.070	0.350	50:50	99:1	0.35
0.1	C	0.314	0.070	0.349	0.162	0.004	0.019	0.152	0.066	0.330	48:52	95:5	0.35
2.2	A	0.366	0.052	0.261	0.255	0.001	0.004	0.111	0.051	0.257	30:70	99:1	0.19
2.4	B	0.344	0.051	0.253	0.242	0.003	0.015	0.102	0.048	0.239	30:70	94:6	0.19
2.4	C	0.470	0.040	0.201	0.371	0.003	0.018	0.099	0.037	0.183	21:79	91:9	0.14
6.4	A	0.385	0.034	0.169	0.262	0.001	0.006	0.123	0.033	0.164	32:68	96:4	0.26
6.6	B	0.363	0.035	0.174	0.242	0.002	0.011	0.121	0.033	0.164	33:67	94:6	0.27
6.7	C	0.387	0.034	0.170	0.260	0.001	0.006	0.127	0.033	0.164	33:67	96:4	0.27
R propellant													
0.1	A	0.309	0.073	0.367	0.121	0.001	0.014	0.188	0.072	0.362	61:39	99:1	0.49
0.1	B	0.309	0.074	0.370	0.129	0.002	0.024	0.180	0.072	0.361	58:42	98:2	0.46
0.1	C	0.319	0.068	0.341	0.143	0.001	0.018	0.176	0.067	0.335	55:45	98:2	0.43
2.3	A	0.346	0.066	0.330	0.187	0.001	0.009	0.159	0.065	0.327	46:54	98:2	0.34
2.5	B	0.316	0.065	0.324	0.158	0.001	0.008	0.158	0.064	0.322	50:50	99:1	0.37
2.5	C	0.378	0.052	0.259	0.231	0.001	0.015	0.148	0.051	0.255	39:61	98:2	0.30
6.5	A	0.341	0.067	0.335	0.145	0.001	0.016	0.196	0.066	0.330	57:43	98:2	0.47
6.6	B	0.352	0.057	0.283	0.164	0.002	0.028	0.188	0.055	0.275	53:47	97:3	0.45
6.7	C	0.424	0.031	0.156	0.249	0.001	0.026	0.175	0.030	0.152	41:59	97:3	0.38

Note. Relative error of the determination of the parameters does not exceeds 15% and is typically ≈10% [31].

TABLE 6

Some Properties and Combustion Parameters of RDX and HMX

Nitramine	ρ, g/cm^3 [5]	T_{melt}, °C, [5]	Q, cal/g [5]	r, mm/sec [34]	L, μm [34]
RDX ($C_3H_6N_6O_6$)	1.82	205	−66	0.5 (0.1 MPa) 5 (2 MPa) 18 (9 MPa)	120 (0.1 MPa) 20 (2 MPa) 15 (9 MPa)
HMX ($C_4H_8N_8O_8$)	1.9	285	−61	0.35 (0.1 MPa) 4 (2 MPa) 10 (7 MPa)	70 (0.1 MPa) 20 (2 MPa) 15 (7 MPa)

Note. ρ is the density, Q is the standard heat of formation, r is the burning rate, L is the thickness of the molten layer; the melting point T_{melt} coincides with the temperature at the beginning of decomposition [5].

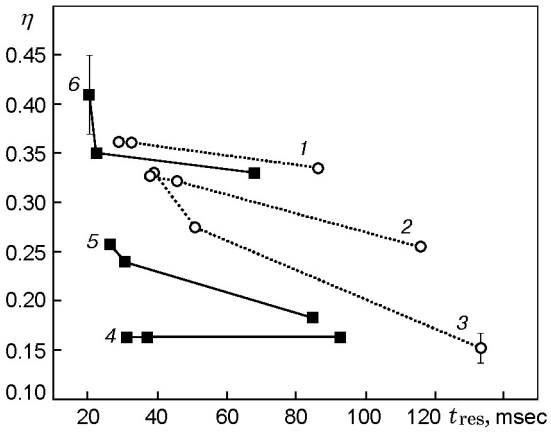

Fig. 6. Dynamics of aluminum burnout from the population of agglomerates of E12 and R propellants (the incompleteness of aluminum combustion η versus the residence time t_{res}): curves 1–3 refer to R propellant at p = 0.1 (1), 2.3–2.5 (2), and 6.5–6.7 MPa (3); curves 4–6 refer to E12 propellant at p = 6.4–6.7 (4), 2.2–2.4 (5), and 0.1 MPa (6).

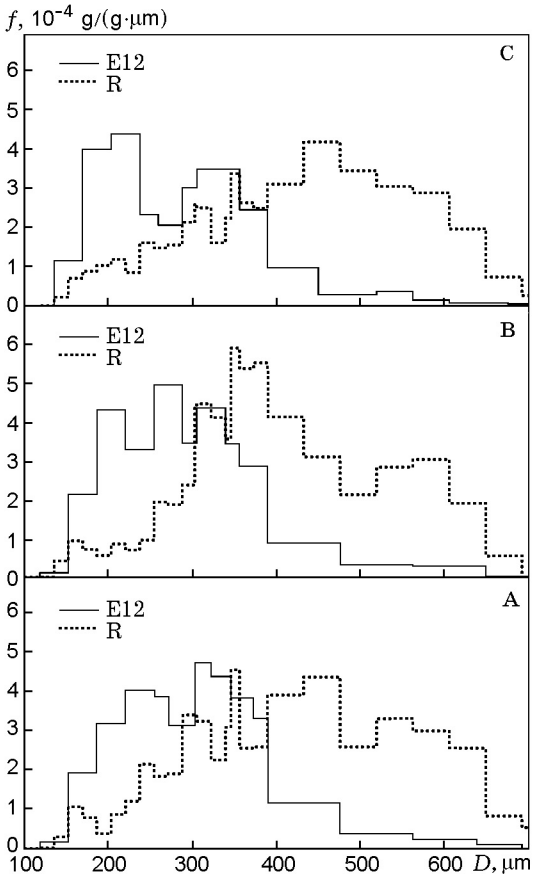

Fig. 7. Mass distributions of agglomerates of E12 and R propellants in the range of sizes of 100–700 μm with a change in the geometry of experiments ($p \approx 2.5$ MPa); the residence time increases in the sequence of the geometry of experiments A→B→C.

An analysis of the data shows that in all cases, the mass distributions of the agglomerates do not undergo considerable changes with distance from the burning surface. The agglomerate mass m_{ag} (column 9 in Table 5) varies more significantly with pressure variation than with a change in the combustion geometry at a given pressure. At the same time, the amount of metallic aluminum in the agglomerates decreases with time (see Fig. 6). The weak change in the agglomerate mass throughout burnout is explained by the fact that the oxide substitutes for metallic aluminum. In other words, part of the oxide formed is not removed into the external flow but remains on the agglomerate. This phenomenon will be discussed below.

We give some data of [24], where the evolution of burning agglomerates of a propellant consisting of 49.5% AP, 21.4% of RDX, 12% HTPB, and 17% Al was studied using a sampling bomb with a rotated drum [35]. In [24], the sample diameter was 6.28 mm, the sample length was 10 mm, and the experiments were

performed with changes in pressure (2.3 or 7 MPa), aluminum particle size (7, 17 or 30 μm), and particle quenching distance (7, 17, ..., 77 mm).

In [24], it was found that the agglomerate size decreased considerably at a rather short distance from the burning surface and then remained almost unchanged. Thus, at $p = 2.3$ MPa, for a quenching distance of 7 mm, the size D_{43} was equal to 510 μm, and for distances of 17–77 mm, D_{43} = 338–405 μm. At $p = 7$ MPa, D_{43} = 303–312 μm for distances of 7 and 17 mm and D_{43} = 191–217 μm for distances of 27–77 mm. In both cases, there is a spread of data in the indicated ranges but not a monotonic decrease of D_{43}. In [24], the variation in the aluminum combustion completeness ξ with increasing quenching distance also had the nature of a spread rather than a monotonic increase. For $p = 2.3$ MPa and distances of 17–77 mm, the average value is $\xi = 0.637 \pm 0.031$, and for $p = 7$ MPa and distances of 27–77 mm, it is $\xi = 0.655 \pm 0.023$. The results for shorter distances are not given in [24].

Comparing the results of [24] with our data, we note the following.

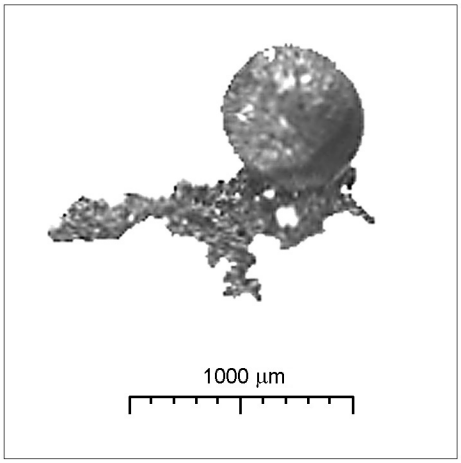

Fig. 8. An agglomerate with adjoining formations of semisintered metal particles, which ensure its retention on the burning surface (R propellant, geometry A, and $p = 0.1$ MPa; a particle from the 450–600 μm fraction).

• In [24], the particles were quenched in a liquid, and in our study, in a cocurrent gas flow. Keeping in mind the length of the initial mixing segment L_{mix} (see Fig. 3), the minimum quenching distance in our experiments can be estimated at 20–30 mm. From the data of [24], at a distance from the surface of 17–27 mm, the agglomerate size D_{43} does not change any more. From our data, the change of D_{43} at a distance of 20–130 mm is also insignificant (within the error).

• The change of D_{43} from 300 to 200 μm (at $p = 7$ MPa) at a distance of 17–27 mm recorded in [24] cannot be explained only by aluminum burnout. The considerable change in the size is probably related to a change in the effective density of the agglomerates [35].

• In [24], no change was observed in the unburned aluminum content with distance from the burning surface. In aggregate with the particle size data, this indicates the cessation of agglomerate combustion under the conditions of [24]. In contrast, under the conditions of our experiments, the agglomerates mostly continue to burn, as is shown by the data in Fig. 6. The only case where the metallic aluminum content is the lowest and does not vary with time occurs for combustion of E12 propellant at $p = 6.5$ MPa under conditions favorable for metal burnout — the maximum pressure and the minimum agglomerate size. This agrees with the results of [36], where it is shown that increasing pressure favors aluminum burnout and that smaller-size agglomerates reach a higher degree of transformation over the same time interval (contain less unburned aluminum) than coarse agglomerates.

• In [24], the agglomerate size D_{43} was in the range of 190–510 μm and their burnout ceased. In our experiments, the burnout of agglomerates with $D_{43} = 290$ μm ceased, and agglomerates with D_{43} = 310–800 μm continued to burn. In addition, there is an apparent (see Fig. 6) difference in the burnout dynamics between the populations of agglomerates of E12 and R propellants. This confirms the conclusion that the burnout process depends on pressure and agglomerate size. It can be assumed that the burnout process also depends on the structure of the agglomerate. One of the main parameters characterizing the state (structure) of an agglomerate is the mass ratio of unburned aluminum and aluminum oxide. It is reasonable to assume that this ratio varies during agglomerate burning and its initial value is determined by the agglomeration process, i.e., it depends on the properties of the propellant and combustion conditions. An analysis of the data of Table 3 for geometry A shows that the metallic aluminum content in 130–600 μm fractions varies with pressure but it has close values for each pressure level. For example, for E12 propellant at $p = 2.2$ MPa, the aluminum content in 130–300, 300–450, and 450–600 μm fractions is 47.8, 47.8, and 47.3%, respectively. A hypothetical explanation for closeness of the aluminum contents in the agglomerates of different sizes leaving the surface is as follows. We suppose that the subsurface propellant

layer is enriched with metal and that aluminum in this layer is subjected to heterogeneous oxidation by the decomposition products of the binder, AP, and nitramine [26]. The degree of aluminum transformation depends on the pressure and structure of the propellant. Detachment of fragments of this layer leads to the formation of agglomerates with the metallic aluminum content corresponding to the state of the layer. Because of the propellant heterogeneity, the layer is inhomogeneous and the burning surface is rough. When the melting point of aluminum is reached on any area of the layer, for example, in an area that protrudes into the gas phase, this locality takes a spherical shape, continuing to be retained on the surface by the "roots" of sintered aluminum particles (Fig. 8). At this stage, the agglomerate can grow because of the absorption of new portions of the metal. The condition for the liftoff of the agglomerate is the disruption of the retaining bond. Ignition of the agglomerate, i.e., transition from heterogeneous oxidation to vapor-phase combustion leads to an immediate liftoff of the agglomerate. However, liftoff can also occur before ignition if the aerodynamic force exerted on the agglomerate by the escaping gas exceeds the force retaining the agglomerate on the surface. The retention force is determined by the strength of the bridge consisting of sintered aluminum particles. An analysis of the balance of the forces in the situation described here is given in [37]. The natural question arises: What determines the strength of the bridge for the propellants studied? A pairwise comparison of the data of Table 3 for E12 and R propellants at $p = 0.1$ and 2.5 MPa for geometry A shows that the metallic aluminum content in the same sieved fractions is mostly lower for R propellant than for E12 propellant. This indicates the more intense condensed-phase aluminum oxidation in the case of R propellant, which is likely due to the fact that RDX begins to react at lower temperature than HMX (see Table 6). In contrast, at $p = 6.5$ MPa, the aluminum content in the 130–900 μm fractions of CCPs is somewhat higher for E12 propellant. This may be attributed to the difference in the burning rate between the propellants ($r = 13$ mm/sec for E12 propellant and $r = 10$ mm/sec for R propellant). With other conditions being equal, the higher the burning rate, the greater the detaching aerodynamic force, which can lead to earlier liftoff of agglomerates with higher contents of unburned aluminum.

The above data suggest that the strength of the retention force increases with increasing completeness of metal oxidation in the subsurface layer. Thus, one may expect that the agglomerate size is larger the higher the oxide content in the agglomerates. Indeed, this correlation occurs in [23] for propellants consisting of 54% AP, 18% of RDX, 16% Al, and 12% HTPB. In [23], 13 propellants of the indicated composition were studied with changes in the particle size of AP (partial replacement of 400 μm particles by 225, 90, or 25 μm particles), the particle size of RDX (full replacement of 100 μm particles by 50 or 15 μm particles), and the aluminum particle size (5 or 15 μm).

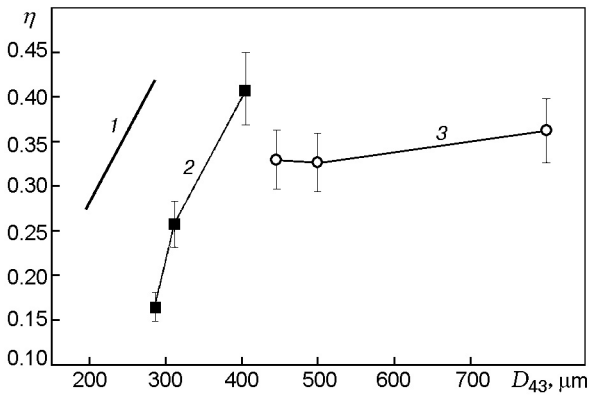

Fig. 9. Incompleteness of aluminum combustion versus agglomerate size: segment 1 is the correlation from [24] for $p = 0.1$–7 MPa; curves 2 and 3 refer to the data of the present study for E12 and R propellants, respectively (sampling in geometry A); the points refer to pressures $p = 6.4$, 2.2, and 0.1 MPa; for all curves, the pressure increases from right to left (η decreases with increasing pressure).

The correlation from [23] plotted as a straight-line segment of the incompleteness of combustion η versus the agglomerate size D_{43} is presented in Fig. 9 along with data for E12 and R propellants. We note that the range of η and D_{43} for E12 and R propellants is much wider than that for 13 propellants in [23]. We recall that η was calculated using not only chemical analysis data (see Table 3) but also mass distributions. In most cases, the agglomerate mass m_{ag} is larger for R propellant than for E12 propellant (see column 9 in Table 5, i.e., during combustion of R propellant, most of the metal participates in the formation of agglomerates. Therefore, different dependences $\eta(D_{43})$ hold for E12 and R propellants, which is due to the behavior of the nitramines in the combustion wave.

Continuing the analysis of the data of Table 3, we note that at a distance from the burning surface (samplings in geometries B and C), the metallic aluminum content in agglomerates in 130–300, 300–450, and 450–600 μm fractions becomes different. This is apparently due to the burnout of the agglomerates. Starting from the burning surface with approximately identical aluminum content, agglomerates of different sizes then evolve differently. On the one hand, large agglom-

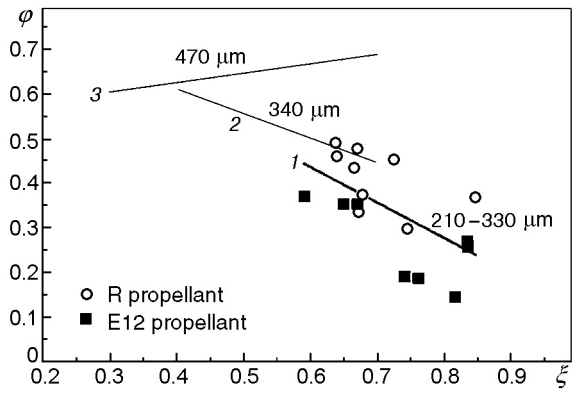

Fig. 10. Effect of the agglomerate size on the dependence $\varphi(\xi)$ for R and E12 propellants: line 1 is an approximation of the entire population of points for E12 and R propellants (samplings in geometries A, B, and C; $p = 0.1$–6.7 MPa; $D_{10} \approx 210$–330 μm) and lines 2 and 3 are the approximating relations from [36] for monodisperse agglomerates with $D_{10} \approx 340$ and 470 μm, respectively.

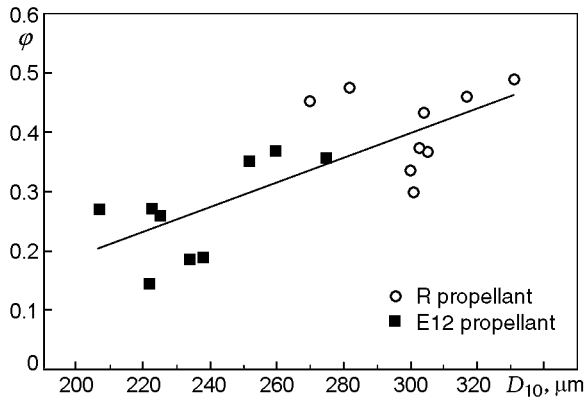

Fig. 11. Dependence $\varphi(D_{10})$ for R and E12 propellants: the curve is an approximation of the entire population of points.

erates are slowly accelerated and are at the quenching distance for a longer time, on the other hand, rate of aluminum burnout (consumption) for them [36] is lower.

Agglomerate Evolution and Oxide Accumulation on the Agglomerate Surface

The accumulation of condensed oxide in the form of a cap on the surface is an important feature of the aluminum particle (and agglomerate) combustion. This feature is usually characterized by a parameter φ that is equal to the ratio of the mass of the oxide accumulated on the burning particle to the total mass of the oxide produced by combustion of this particle [36].

In this study, the representativeness of the samplings is close to 100%, which enables the mean value of φ to be calculated for the population of agglomerates (column 14 in Table 5).

Following [36], we consider the combustion completeness ξ as a parameter that characterizes the state of an agglomerate, ignoring the factors influencing the measured value of ξ. Figure 10 gives the dependence $\varphi(\xi)$ for E12 and R propellants. The points on the plot correspond to all experiments performed ($D_{10} \approx 210$–330 μm, $p = 0.1$–6.5 MPa, and geometries A, B, and C); straight line 1 is an approximation of the entire set of data by the linear dependence $\varphi(\xi) = (0.91 \pm 0.18) - (0.79 \pm 0.24)\xi$ for the coefficient of determination $R^2 = 0.40$. Figure 10 also gives approximating dependences $\varphi(\xi)$ for monodisperse agglomerates with $D \approx 340$ μm at $p = 0.19$–6.2 MPa (straight line 2) and with $D \approx 470$ μm at $p = 0.1$–7 MPa (straight line 3) from [36]. A comparison of graphs 1–3 shows that the agglomerate size is a key physical factor that governs the mass ratio of the accumulated and removed oxide.

Figure 11 presents the dependence of the parameter φ on the agglomerate size D_{10}. The agglomerate sizes for E12 and R propellants differ significantly ($D_{10} \approx 210$–280 μm for E12 and $D_{10} \approx 270$–330 μm for R). The arrangement of the points in Fig. 11 is such that one can speak of a unified dependence $\varphi(D_{10})$ for both propellants. The linear approximation of the dependence $\varphi(D_{10})$ for the entire population of points (straight line in Fig. 11) has the form $\varphi(D_{10}) = -(0.22 \pm 0.12) + (0.0020 \pm 0.0004)D_{10}$ (the coefficient of determination is $R^2 = 0.58$).

The result obtained indicates that the evolution of agglomerates for E12 and R propellants obeys the same laws. In other words, if they had the same size, their burnout would be identical under identical conditions.

CONCLUSIONS

In the pressure range of 0.1–6.5 MPa, E12 and R propellants are characterized by severe aluminum agglomeration, which is due to features of their formulations (35% of coarse nitramine in combination with an active binder).

Although the burning rates of the propellants under identical conditions are comparable and the HMX particle size in E12 propellant is approximately 1.5 times larger than the RDX particle size in R propellant, the RDX-based propellant is characterized by more severe agglomeration: the agglomerate size and mass are larger and the completeness of aluminum combustion is

lower. The formation of larger-size agglomerates for the nitramine of smaller particle size is inconsistent with the pocket agglomeration concept and is related to the behavior of HMX and RDX in the combustion wave. The reaction of RDX begins at a lower temperature. This presumably leads to more active aluminum oxidation in the condensed phase in the heterogeneous regime and the resulting oxide contributes to the retention of agglomerates on the surface.

The macrokinetic regularities of the burnout of the population of agglomerates (i.e., the rate of aluminum consumption through transformation to the oxide) are different for E12 and R propellants. In the experiments performed at a pressure of 6.5 MPa, a fairly high completeness of aluminum combustion $\xi \approx 0.85$ was observed for both propellants. However, for E12 propellant, the indicated value was reached in approximately 30 msec, and for R propellant, in 130 msec. The observed differences in the burnout dynamics are due to differences in the initial parameters of agglomerates — the size and aluminum content at the moment of detachment from the surface.

During agglomerate combustion, the resulting aluminum oxide is partly retained on the agglomerate. Because of the substitution of the oxide for aluminum, the agglomerate mass distributions vary weakly with time in the range of parameters studied, despite the significant variation in the completeness of aluminum combustion. The ratio of the mass of the oxide accumulated on the burning particle to the total mass of the oxide formed depends on the size of the burning particle.

I thank O. N. Zhitnitskaya, T. D. Fedotova, and A. G. Kir'yanova for particle-size and chemical analyses, and V. E. Zarko, L. G. Gusachenko, and A. G. Tereshchenko for fruitful discussions.

This work was supported by EOARD (Contract No. F61708-97-W0197), an INTAS (Grant No. 93-2560ext), and an International Science and Technology Center (Project No. 2358).

REFERENCES

1. V. F. Komarov and V. A. Shandakov, "Solid fuels, their properties and applications," *Combust., Expl., Shock Waves*, **35**, No. 2, 139–143 (1999).
2. G. Lengellé, J.-R. Duterque, J.-C. Godon, and J.-F. Trubert, "Solid propellant combustion — physical aspects," in: *AGARD Lecture*, Series 180: *Combustion of Solid Propellants*, NATO Edition (1991), pp. 3-1–3-25.
3. L. V. Zabelin, R. V. Gafiyatullin, and L. R. Guseva, "Environmental aspects of the disposal of solid-rocket propellant motor charges," *Khim. Rossiya*, February, 4–7 (1999).
4. E. Yu. Orlova and V. F. Zhilin, *HMX — a Heat-Resistant Explosive* [in Russian], Nedra, Moscow (1975).
5. M. L. Chan, R. Reed (Jr.), and D. A. Ciaramitaro, "Advances in solid propellant formulations, " in: V. Yang, T. B. Brill, and Wu-Zhen Ren (eds), *Progress in Astronautics and Aeronautics*, Vol. 185: *Solid Propellant Chemistry, Combustion, and Motor Interior Ballistics*, Chapter 1.7, AIAA Inc., Reston (2000), pp. 185–206.
6. T. L. Boggs, "The thermal behavior of RDX and HMX," in: K. K. Kuo and M. Summerfield (eds.), *Progress in Astronautics and Aeronautics*, Vol. 90: *Fundamentals of Solid Propellant Combustion*, AIAA, New York (1984), pp. 121–175.
7. R. A. Fifer, "Chemistry of nitrate ester and nitramine propellants," *ibid*, pp. 177–237.
8. N. E. Ermolin and V. E. Zarko, "Mechanism and kinetics of the thermal decomposition of cyclic nitramines (review)," *Combust., Expl., Shock Waves*, **33**, No. 3, 251–271 (1997).
9. *J. Propuls. Power*, **11**, No. 4 (1995).
10. *J. Propuls. Power*, **15**, No. 6 (1999).
11. V. N. Simoneneko, A. B. Kiskin, V. E. Zarko, and A. G. Svit, "Special features of nitramine combustion at atmospheric pressure," *Combust., Expl., Shock Waves*, **33**, No. 6, 685–688 (1997).
12. N. E. Ermolin and V. E. Zarko, "Investigation of the properties of a kinetic mechanism describing the chemical structure of RDX flames. II. Construction of a reduced kinetic scheme," *Combust., Expl., Shock Waves*, **37**, No. 3, 247–255 (2001).
13. A. A. Zenin, V. M. Puchkov, and S. V. Finyakov, "Characteristics of HMX combustion waves at various pressures and initial temperatures," *Combust., Expl., Shock Waves*, **34**, No. 2, 170–177 (1998).
14. O. P. Korobeinichev, L. V. Kuibida, and V. Zh. Madirbaev, "Investigation of the chemical structure of the HMX flame," *Combust., Expl., Shock Waves*, **20**, No. 3, 282–285 (1984).
15. N. E. Ermolin, O. P. Korobeinichev, L. V. Kuibida, and V. M. Fomin, "Processes in RDX flames," *Combust., Expl., Shock Waves*, **24**, No. 4, 400–407 (1988).
16. O. G. Glotov, V. V. Karasev, V. E. Zarko, and A. G. Svit, "Burning of single crystals and pressed tablets of RDX," in: *Energetic Materials: Reactions of Propellants, Explosives, and Pyrotechnics*, Proc. of the 34th Int. Annual Conf. of ICT, Karlsruhe, Germany (2003), pp. 47-1–47-15.
17. J. Duterque and G. Lengellé, "Combustion mechanisms of nitramine-based solid propellants with additives," *J. Propuls. Power*, **6**, No. 6, 718–726 (1990).
18. W. H. Hsieh and W. Y. Li, "Combustion behavior and thermochemical properties of RDX-based solid propellants," *Propellant, Explos., Pyrotech.*, **23**, No. 3, 128–136 (1998).

19. A. P. Denisyuk, Yu. G. Shepelev, D. L. Rusin, and I. V. Shumskii, "Effect of RDX and HMX on the efficiency of catalysts for double-base propellant combustion," *Combust., Expl., Shock Waves*, **37**, No. 2, 190–196 (2001).
20. Rm. Muthiah, T. L. Varghese, S. S. Rao, et al., "Realization of an eco-friendly solid propellant based on HTPB–HMX–AP system for launch vehicle applications," *Propellants, Explos., Pyrotech.*, **23**, No. 2, 90–93 (1998).
21. W. N. Brundige and L. H. Caveny, "Low burning rate aluminized propellants in acceleration fields," *AIAA J.*, **22**, No. 5, 638–646 (1984).
22. S. Suzuki and M. Chiba, "Combustion efficiency of aluminized propellants," AIAA Paper No. 89-2309, 1–8 (1989).
23. T.-K. Liu, H.-C. Perng, S.-P. Luh, and F. Luh, "Aluminum agglomeration in AP/RDX/Al/HTPB propellant combustion," *J. Propuls. Power*, **8**, No. 6, 1177–1184 (1992).
24. T.-K. Liu and C.-F. Hsieh, "Analysis of agglomerate size from burning aluminized an AP/RDX/HTPB propellants in quench bomb," *J. Propuls. Power*, **12**, No. 5, 995–998 (1996).
25. S.-P. Luh, T.-K. Liu, H.-C. Perng, and F. Liu, "Pocket model application to the combustion of AP/RDX/Al/HTPB propellant," AIAA Paper No. 95-3110, 1–6 (1995).
26. Zhu Ji and Li Shufen. "Aluminum oxidation in nitramine propellant," *Propellants, Explos., Pyrotech.*, **24**, No. 4, 224–226 (1999).
27. O. G. Glotov, V. E. Zarko, V. V. Karasev, and M. W. Beckstead, "Aluminum agglomeration in solid propellants: Formulation effects," in: *Propellants, Explosives, Rockets, and Guns*, Proc. of the 2nd Int. High Energy Materials Conf. and Exhibit, IIT, Madras, Chennai, India, December 8–10 (1998), pp. 131–137.
28. O. G. Glotov and V. E. Zarko, "Condensed combustion products of aluminized propellants," *Trans. Aeronaut. Astronaut. Soc. Rep. China*, **34**, No. 3, 247–256 (2002).
29. O. G. Glotov and V. E. Zarko, "Condensed combustion products of aluminized propellants. I. A technique for investigating the evolution of disperse-phase particles," *Combust., Expl., Shock Waves*, **31**, No. 1, 72–78 (1995).
30. T. D. Fedotova, O. G. Glotov, and V. E. Zarko, "Chemical analysis of aluminum as a propellant ingredient and determination of aluminum and aluminum nitride in condensed combustion products," *Propellants, Explos., Pyrotech.*, **25**, No. 6, 325–332 (2000).
31. O. G. Glotov, "Condensed combustion products of aluminized propellants. II. Evolution of particles with distance from the burning surface," *Combust., Expl., Shock Waves*, **36**, No. 4, 476–488 (2000).
32. O. G. Glotov, V. E. Zarko, V. V. Karasev, and M. W. Beckstead, "Effect of binder on the formation and evolution of condensed combustion products of metallized solid propellants," in: *Combustion and Detonation*, Proc. of the 28th Int. Annual Conf. of ICT, Karlsruhe, Germany (1997), pp. 75-1–75-14.
33. A. Afifi and S. Azen, *Statistical Analysis: A Computer Oriented Approach*, Academic Press, New York (1979).
34. A. Zenin, "HMX and RDX: Combustion mechanism and influence on modern double-base propellant combustion," *J. Propuls. Power*, **11**, No. 4, 752–758 (1995).
35. Yu. V. Frolov, P. F. Pokhil, and V. S. Logachev, "Ignition and combustion of aluminum powder in high-temperature gaseous media and in a composition of heterogeneous condensed systems," *Combust., Expl., Shock Waves*, **8**, No. 2, 168–187 (1972).
36. O. G. Glotov, V. E. Zarko, V. V. Karasev, et al., "Macrokinetics of combustion of monodisperse agglomerates in the flame of a model solid propellant," *Combust., Expl., Shock Waves*, **39**, No. 5, 552–562 (2003).
37. V. Ya. Zyryanov, Model for predicting agglomeration in combustion of metallized systems," in: *Combustion of Condensed Systems*, Joint Institute of Chemical Physics, Russian Academy of Sciences, Chernogolovka (1986), 59–62.